



# Evolution characteristics of fracture volume and acoustic emission entropy of monzogranite under cyclic loading

Liyuan Liu · Zhou Zhang · Tao Wang · Sheng Zhi · Jiong Wang

Received: 12 October 2023 / Accepted: 11 January 2024  
© The Author(s) 2024

**Abstract** The volume evolution behavior of rock fissures and the characteristics of acoustic emission under cyclic loading are critical for rock stability analysis. To study the volume change behavior of monzogranite fissures and the characteristics of acoustic emission signals under cyclic loading, we selected samples of monzogranite at – 1600 m from a gold mine located in the Jiaodong Peninsula at a depth of – 1600 m and investigated the samples using triaxial cyclic loading—unloading tests and acoustic emission monitoring. As the volume change behavior of the monzogranite fissures and acoustic emission signals were monitored and recorded, the calculated fracture volume strain ratio coefficient and acoustic emission entropy value were proposed to describe the evolution process of fissures inside the rock. The research results showed that the volume strain ratio curve of the rock fractures exhibited a logarithmic variation characteristic during the cyclic loading and unloading, and the fracture volume strain ratio

better reflected the relative scale of the internal fracture strain in the rock to the total volume strain. The acoustic emission entropy value reflected the crack evolution behavior during the loading and failure processes, which was a rapid decline in the initial stage of loading and a rapid upward trend in the failure stage. The observed “V”-shaped change in the acoustic emission entropy can be used as an early warning for rock failure. The research results can provide theoretical guidance for rock stability analysis.

## Highlights

- (1) The fracture volume strain ratio coefficient, defined as the scale of the internal fracture strain to the total volumetric strain, is proposed to describe the evolution process of fissures inside the rock during cyclic loading. Comparing to fracture strain, it is novel and rational to use this dimensionless coefficient in rock failure analysis.
- (2) The acoustic emission entropy is calculated by acoustic emission amplitude to visualize crack development since the process of crack development and expansion which is a nonlinear process from disorder to order. A “V”-shaped change in the acoustic emission entropy is discovered and can be used as an early warning indicator of rock failure.
- (3) As confining pressure rises up, the mode of failure in monzogranite transitions from tension to

---

L. Liu · Z. Zhang · T. Wang (✉) · J. Wang  
School of Civil and Resources Engineering, University  
of Science and Technology Beijing, Beijing 100083, China  
e-mail: tao.w@ustb.edu.cn

Z. Zhang  
Shanxi Yingrun New Energy Company Limited,  
Taiyuan 030000, China

S. Zhi  
Department of Equity Investment, China Huarong  
International Holdings Limited, Hong Kong, China

shearing, and correspondingly the volumetric strain ratio curve of the fracture changes from flat to upward sloping.

**Keywords** Cyclic load · Monzogranite · Fracture volume · Fracture volume strain ratio · Acoustic emission entropy

## 1 Introduction

As social productivity improves, people's demand for mineral resources increases, shallow mineral resources are gradually exploited and exhausted, and deep mineral resource mining gradually becomes more common. The deformation and damage caused by cyclic loading of rocks under deep burial or high in-situ stress is becoming more critical (Taheri et al. 2016; Wang et al. 2021; Erarslan 2016; Hoek and Martin 2014; Erarslan 2013). The superimposed evolution of micro-cracks in the rock mass results in macroscopic damage to the surrounding rock mass in deep underground engineering. Therefore, it is crucial to understand the evolution of cracks in rock to ensure the stable state of the surrounding rock mass, especially during cyclic loading.

Recently, experts and scholars in the field of rock mechanics have intensively studied the evolution characteristics of rock fracture under cyclic loading (Ma et al. 2013; Liu et al. 2022; Qiu et al. 2014; Liu et al. 2022). Meng studied the deformation and volume expansion characteristics of rock under different confining pressures as well as cyclic loading and unloading conditions, and the author found that confining pressure significantly affects the expansion of micro-cracks in rock (Meng et al. 2021). Xiao studied the internal fracture and deformation law of rock under cyclic loading and unloading conditions using the rock residual strain method (Xiao et al. 2009). Momeni analyzed the stress–strain relationship of granite under different peak loads and different loading amplitudes under cyclic loading. The author observed three-stage characteristics in the deformation and failure process of the rock (Momeni et al. 2015). Ghamgosar studied the development behavior of cracks in rock under split conditions and found that more high-density cracks can be generated in the rock under the action of cyclic loading (Ghamgosar

and Erarslan 2016). Xu propose a two-dimensional meso-scale elasto-plastic damage model to simulate the fatigue behavior of rock during cyclic loading. And they found that specimen failure occurs once the cumulative axial deformation under cyclic loading reaches the axial strain that corresponds to the post-peak phase of the stress–strain curve from a conventional uniaxial test simulation (Xu et al. 2021). Zhou used computed tomography imaging technology and digital image correlation testing technology to analyze the expansion and evolution behavior of the internal fractures of a rock under the action of load. The author found that the deformation and failure process of the rock can be divided into five stages (Zhou et al. 2020). Zhang used acoustic emission and high-speed camera technology to find that the initiation and development of rock cracks were consistent with the change in the crack inclination angle (Zhang et al. 2019). Ma systematically examine the influence of fissure angles, lengths and positions on the mechanical response. They found that the burst tendency of composite specimens can be effectively reduced by a fissure in either the weak (lower, SWL) or strong (upper, SWU) layers. However, the effectiveness of the fissure depends on the angle and length of the fissure (Ma et al. 2023). Ghasemi used the fluorescent labeling method to identify the initial fractures in a rock as intergranular and transgranular fractures, and the intergranular fracture expansion under load eventually caused rock failure (Ghasemi et al. 2020). Liu used the dual-damage constitutive model to study the damage and fracture mechanism of deep surrounding rock under high confining pressure (Liu et al. 2020). For the research on the characteristics of acoustic emission signals during the rock cyclic loading and unloading stages, Ji found that under the triaxial test of cyclic loading and unloading of monzonitic granite rock samples, the distribution of the characteristic parameters of granite rock acoustic emission signals has four variation characteristics stages (Ji et al. 2012). Harte analyzed the relationship between information entropy and system stability and used information entropy for earthquake prediction (Harte and Vere-Jones 2005). Bressan claimed that the evolution of entropy value is a description of the expansion process of a thermodynamic system from disorder to order (Bressan et al. 2017). Ju used industrial CT to achieve fracture description in rock deformation and failure engineering under different

confining pressures (Ju et al. 2018). Cai found that the development process of rock fracture can be divided into three stages: fracture initiation, fracture expansion and fracture acceleration (Cai et al. 2004). Duan studied the fracture volume variation of Longmaxi rock under uniaxial compression and found that the fracture volume variation presents two stages of steady growth and accelerated jet expansion (Duan et al. 2019). Chen's study found that the higher the confining pressure, the larger the volume strain of fracture during rock fracture (Chen et al. 2020). Zhang found that the variation of acoustic emission energy rate could reflect the development of rock cracks, and when the AE energy rate was high, the cracks inside the sample gradually increased (Zhang et al. 2006). Akdag found that the AE energy rate corresponded well with the stage of rock compression and deformation, and the AE energy rate could reflect the fracture characteristics during rock deformation and failure (Akdag et al. 2021).

At present, most of the research results focus on the change law of single parameter of rock specimen surface and fracture volume strain, lacking of considering the influence of rock volume change on fracture volume development. In fact, deep stratum rocks are affected by excavation, rock stress field is in the process of dynamic adjustment, and rock volume change has a direct control effect on fracture expansion.

Therefore, the research focus of this paper is to investigate the fracture volume evolution law of monzogranite under cyclic loading, and then to describe the development of cracks in rock samples by introducing fracture volume strain ratio coefficient. This parameter can reflect the variation of fracture volume strain and its relation to the total volume strain of rock samples during loading failure process, and establish AE entropy to describe the development characteristics of fractures in rock. The results are of great significance for rock engineering stability analysis.

## 2 Experimental scheme design

The experimental rock samples were obtained from the monzogranite at a depth of -1600 m in a gold mine located in the Jiaodong Peninsula. The core

column of the collected samples was processed into a cylindrical standard specimen of 50 mm and 100 mm, the allowable deviation of the height and diameter of the rock samples was 3 mm, and the allowable deviation of the unevenness of the two ends of the rock samples was 0.05 mm.

The experimental mechanical loading system was a TAW-2000 rock triaxial rigidity testing machine and a PCI-2 acoustic emission instrument located at the University of Science and Technology Beijing. The experimental instruments are shown as Fig. 1. The resonant frequencies of the acoustic emission probes used for the experiment were 55 kHz and 150 kHz, respectively. Both the pre-gain and the threshold value were 40 dB.

Loading scheme design: At the beginning of the experiment, the testing machine was preloaded by axial pressure at 500 N/s until 5 MPa. It should be noted that the unloading stress is set to 5 MPa to ensure that the indenter of the testing machine is in a close contact with the rock sample. After stabilizing the data, they were cleared and changed to deformation control data, and the deformation rate was 0.01 mm/min. Rocks from a gold mine at a depth of -1600 m are characterized as high-strength and high-hardness. Consequently, the rock samples obtained from the mine had high strength and hardness, and the uniaxial compressive strength reached 220 MPa. The first axial loading was at 100 MPa. The initial load is set to 100 MPa to prevent fatigue damage due to excessive cyclic loading under low stress, while also avoiding significant acoustic emission. To ensure that the experiment can be conducted between seven and nine cycles before the rock sample failure, the loading rate was kept constant, and the stress increase of cyclic loading was 20 MPa before the rock sample failure. Three groups of cyclic loading and unloading experiments were set under different confining pressures (10 MPa, 20 MPa, and 30 MPa). When the target loading stress of each cycle was reached, the samples were unloaded until the stress decrease to 5 MPa, then the next cycle of loading was performed till the specimen failed. The corresponding stress-strain curves and fracture volume strain curves are shown in Figs. 2 and 3.

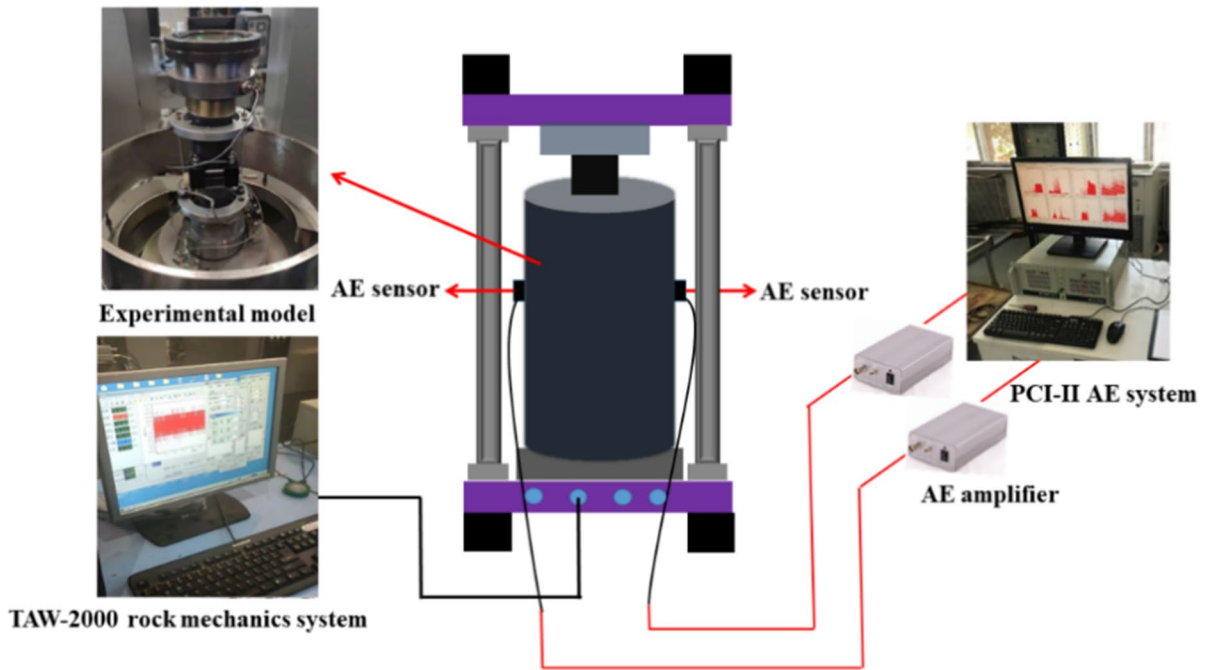


**Fig. 1** Schematic of experimental apparatus

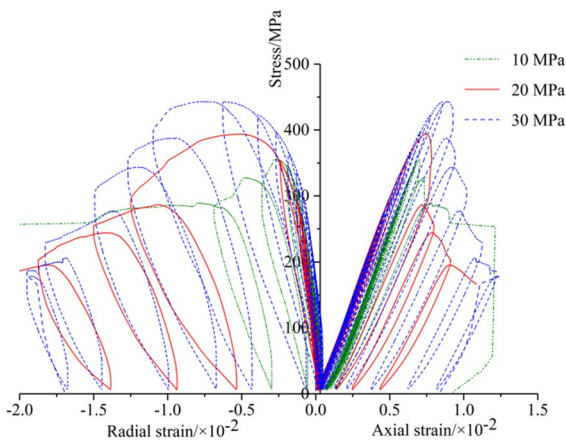


**Fig. 2** The monzogranite’s stress–strain curves under cyclic loading and unloading with different confining pressures

### 3 Deformation characteristics of monzogranite

#### 3.1 Evolution of fissure volume strain ratio coefficient

The initiation and evolution of fractures in the rock changed the rock physical and mechanical

properties, and the volume strain of the fracture is an important parameter for describing the fracture evolution during cyclic loading and unloading. Total rock volume strain is equal to the elastic volume strain plus fracture volume strain (Erarslan 2016; Liu and Dai 2021), as follows:

$$\epsilon_v = \epsilon_{ve} + \epsilon_{vc}, \tag{1}$$

where  $\epsilon_v$  is the total volume strain,  $\epsilon_{ve}$  is the elastic volume strain, and  $\epsilon_{vc}$  is the crack volume strain.

The total volume strain of the rock sample can be determined using Eq. (2):

$$\epsilon_v = \epsilon_1 + 2\epsilon_3, \tag{2}$$

where  $\epsilon_1$  is the axial strain, and  $\epsilon_3$  is the hoop strain.

The volume strain of the rock sample elastic body can be determined using Eq. (3):

$$\epsilon_{ve} = \frac{1 - 2\nu}{E}(\sigma_1 + 2\sigma_3), \tag{3}$$

where  $\nu$  is the Poisson’s ratio in the elastic stage,  $E$  is the elastic modulus,  $\sigma_1$  is the maximum principal stress, and  $\sigma_3$  is the minimum principal stress.

The proportion of the volume strain of the rock sample fractures can be calculated using Eq. (4):

$$F = \frac{\epsilon_{vc}}{\epsilon_v}, \tag{4}$$

where  $F$  is the proportion coefficient of the fracture volume strain, which is the proportion of the fracture volume strain in the rock to the total volume strain and describes the relative scale of the fracture volume strain in the rock to the total volume strain.

The variation characteristics of the volume strain ratio of the monzogranite fissures under different confining pressures were obtained according to Eq. (4). The lower the confining pressure is, the weaker the lateral deformation constraint of the rock is. To better describe the fracture development behavior inside the rock, the volume strain curve of the rock sample fractures under 10-MPa confining pressure was used for analysis and investigation. After the initial cyclic unloading stage, the fracture volume strain curve of the rock sample had obvious residual fracture volume strain because the original fractures of the rock were compacted and closed during the initial cyclic loading stage. The fractures in the rock were completely compacted and closed, and the change rule of the fracture volume strain ratio curve in the later period was roughly the same. Therefore, the representative fracture volume strain ratio curve under the first, second, and fourth cycles was analyzed, as shown in Figs. 3 and 4.

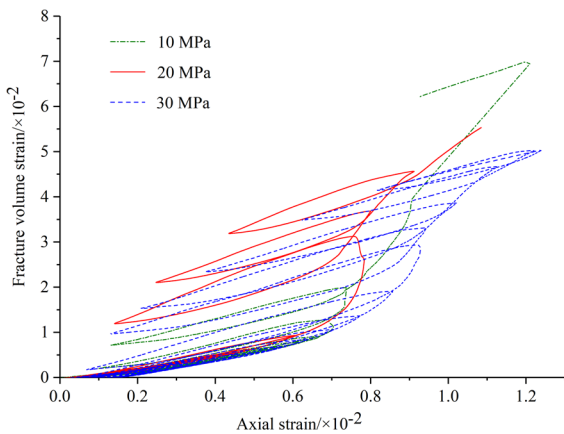


**Fig. 3** Volume strain curves of monzogranite fractures under different confining pressures

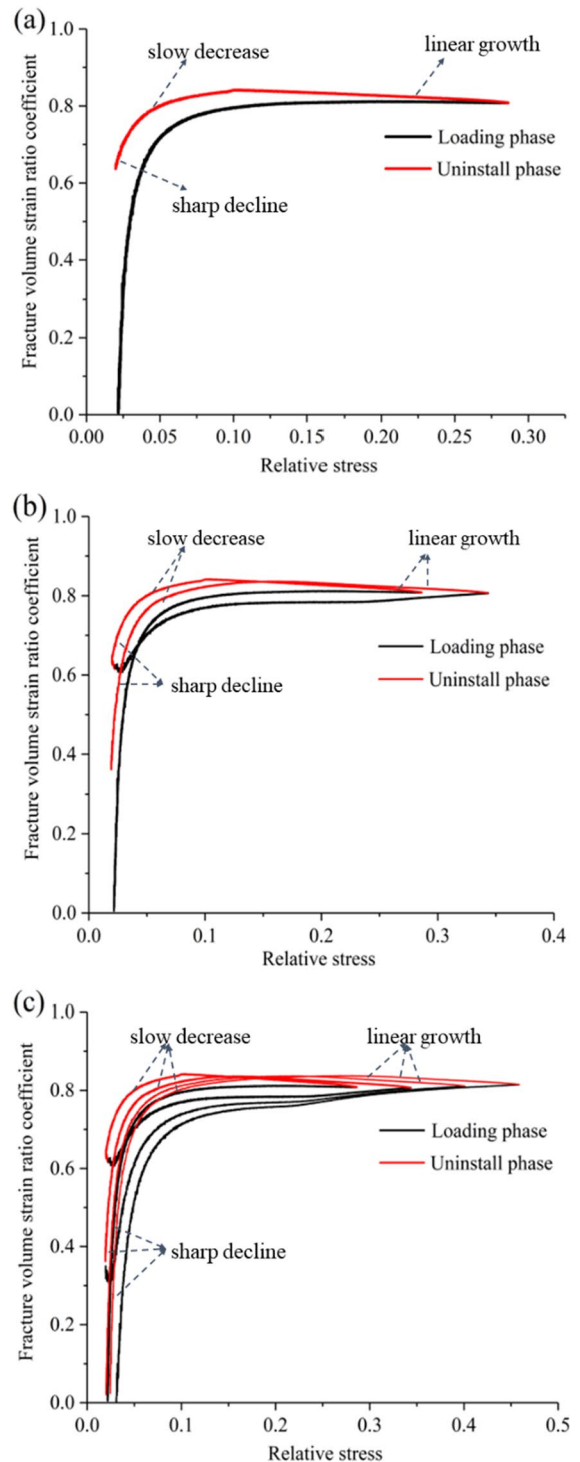


**Fig. 4** Fracture volume strain ratio coefficient under the first, second, and fourth cyclic loads at a confining pressure of 10 MPa: **a** First cycle; **b** Second cycle; **c** Fourth cycle

The ratio of the fracture volume strain to the total volume strain was determined by the ratio of the fractured volume strain to the total volume strain, which can show the relative scale of the fractured volume strain to the total volume strain under different stress states. Relative stress is defined as the ratio of stress to peak stress at different states. Figures 4 and 5 show that under different stress states, fracture volume strain ratio coefficient curve of the monzogranite presented a logarithmic change. The unloading process has three stages: linear growth, slow decrease, and sharp decline.

In the cyclic loading stage of the rock sample, when the relative stress was between 0 and 0.05, the stage was the crack closure stage. The cracks and pores inside the rock were compressed and closed under the action of pressure, and the volume strain ratio of the crack was from 0.6 to 0.7, showing that the rock deformation in this stage was mainly fractured compaction deformation. As the stress level increased, the elastic deformation gradually increased, and the growth rate of the fracture volume strain ratio gradually decreased, stabilizing between 0.8 and 0.85. This behavior indicates that the fracture volumetric and elastic volume strains accounted for the relative volume strain during the loading process. The scale was stable and unchanged, but the fracture volume strain accounted for the main part. When the relative stress level was greater than 0.4, cracks were gradually formed in the rock. Correspondingly, the volume strain ratio of the cracks increased slowly, indicating that the cracks in the rock continued to develop. Meanwhile, the opening degree of the cracks in the rock sample increased under the load, and the volumetric and elastic strains of the cracks increased simultaneously. This stage is the fissure stable development stage.

During the cyclic unloading stage of the rock sample, the volume strain ratio of the fracture increased linearly as the stress level decreased, showing that the elastic deformation inside the rock recovered at first. Then, the volume strain of some uncompacted fractures recovered, as shown in Fig. 4a. When the stress level was unloaded to less than the crack initiation stress, the cracks were gradually closed, the volume strain ratio of the cracks decreased nonlinearly, and

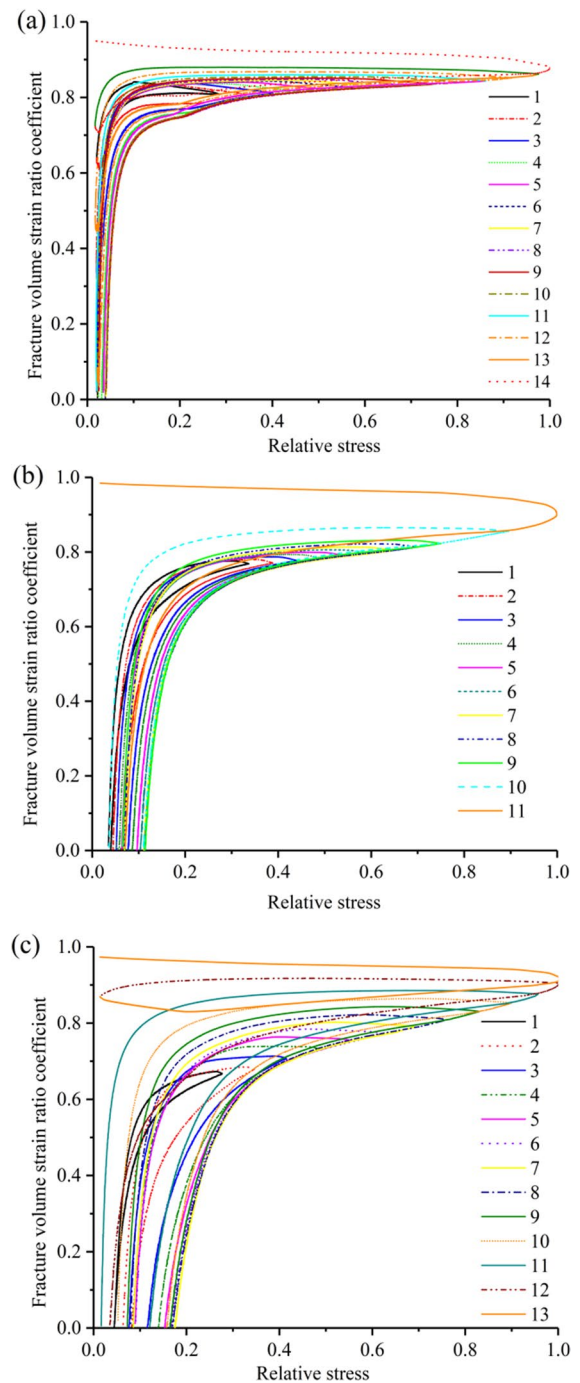


**Fig. 5** Fracture volume strain ratio coefficient of monzogranite under different confining pressures: **a** Confining pressure: 10 MPa; **b** Confining pressure: 20 MPa; **c** Confining pressure: 30 MPa

the relative scale of the total rock volume strain gradually decreased. Finally, the volume strain ratio of the cracks was 0.63, indicating that the sample contained volume strains of compacted fractures. This phenomenon showed that the internal fractures in the rock were compacted and closed after one cyclic loading, and the volume of the closed fractures accounted for 63% of the total volumetric deformation under the stress state.

As the number of cycles increased, the proportion coefficient of the fracture volume strain increased gradually under the same stress level, indicating that the relative scale of the fracture volume strain in the rock to the total volume strain continuously expanded. The fractures in the rock were constantly sprouting and developing, and the damage in the rock was constantly increasing. When the stress level reached the peak stress, the proportion of the fracture volume strain was close to 1, indicating that the deformation at this time was mainly caused by the fracture strain, and the rock was damaged.

### 3.2 Fracture morphology analysis

To characterize the fracture development inside granite rocks under different confining pressures, the failure map of monzogranite samples under different

confining pressures and the scanning electron microscope images of the fracture surface of the rock samples are presented in Figs. 6 and 7.

Figures 6 and 7 show that the monzogranite samples mainly had two failure modes: shearing and tensioning. Under the confining pressure of 10 MPa, the rock sample was mainly damaged by tension: longitudinal tearing cracks were initiated, and the bottom of the rock sample peeled off. At this time, the tensile strength of the rock sample is higher, so it fails in tension. The micro-cracks were mainly concentrated on both sides of the main crack, and many cluster fractures were inside the rock sample. The inclusion distribution was uneven, and the number of ruptured inclusions increased considerably along the main crack direction. The failure mode of the rock sample under the confining pressure of 20 MPa was the combined tension and shear failure modes. A bulging crack occurred in the middle of the rock sample. The failure crack of the rock sample was mainly shear failure, and the number of secondary cracks was considerably reduced. Under the confining pressure of 30 MPa, the rock sample suffered shear damage where the internal intergranular cracks and pores developed in the rock. With the increase of confining pressure, the tensile strength of the rock sample decreases, while the shear strength increases. When the shear stress component exceeds the tensile stress

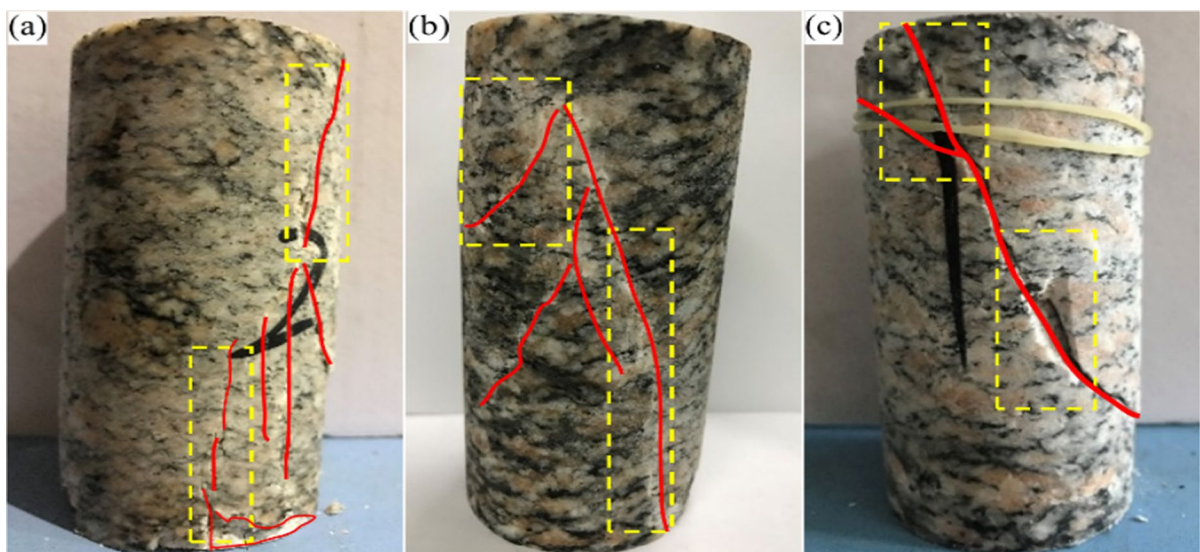


**Fig. 6** Failure patterns of rocks under different confining pressures: **a** Confining pressure: 10 MPa; **b** Confining pressure: 20 MPa; **c** Confining pressure: 30 MPa

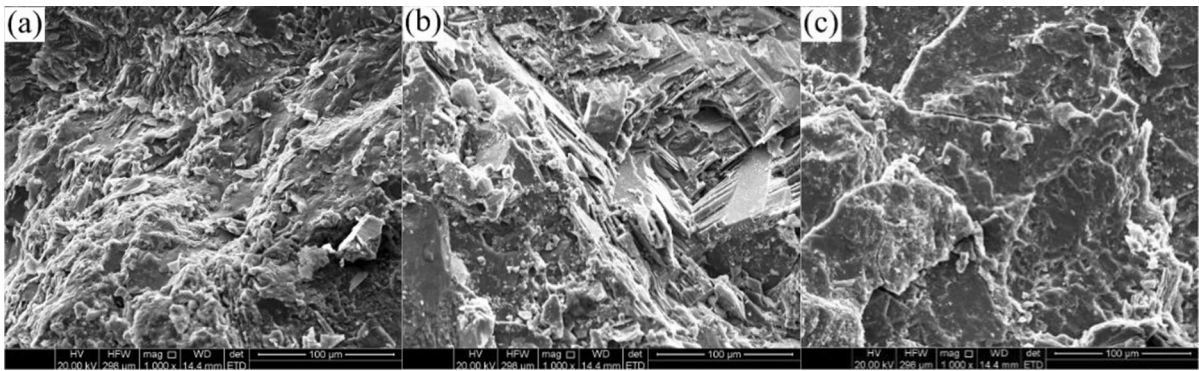


**Fig. 7** Cross-section morphology of rocks under different confining pressures: **a** Confining pressure: 10 MPa; **b** Confining pressure: 20 MPa; **c** Confining pressure: 30 MPa

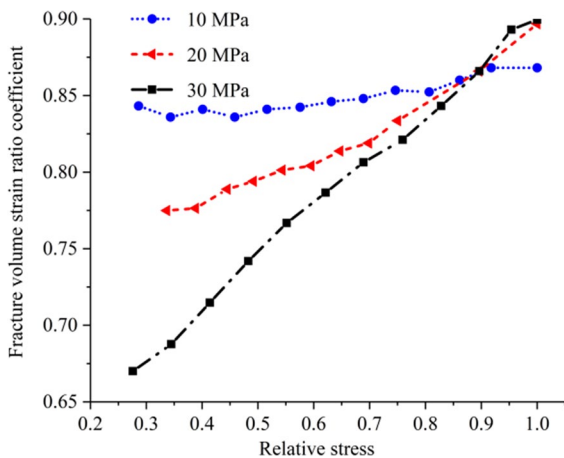


**Fig. 8** Proportion coefficient of volume strain of monzogranite fractures under different confining pressures

component, the rock sample fails in shear. The volume strain ratio of the fractures at the upper limit stress of the rock sample under the 30 MPa confining pressure steadily increased, which resulted from the random development of new micro-cracks and pores inside the rock. The scale of developed fractures and pores did not increase until a certain range because of the high-confining-pressure constraint. The increase in cyclic stress generated sufficient new pores and cracks in the rock sample, making the crack volume grow steadily while an obvious directionality appeared along the shear failure surface. Under the low confining pressure, the confinement effect of the confining pressure was not obvious, the scale of

randomly developed fractures and pores in the rock continued to develop, and the continuous friction between the fracture surfaces produced numerous fractured inclusions and micro-cracks; the volume strain ratio of the fractures fluctuated and did not substantially increase, as shown in Fig. 8.

### 3.3 Characteristics of AE entropy

Entropy is an indicator used for describing system complexity and disorder. The acoustic emission entropy value can be used to describe the distribution of acoustic emission amplitude and show crack development (Harte and Vere-Jones 2005; Bressan et al. 2017) since the process of crack development and expansion in rock mass is a nonlinear process from disorder to order. When fractures in rocks develop into fractures of the same scale, the acoustic emission amplitude distribution is typically relatively close, and the entropy value is large; when the internal fractures in rocks develop into fractures of different scales, the acoustic emission amplitude distribution is wider, and the entropy value is low. Currently, few studies are using the acoustic emission entropy theory to study crack evolution behavior during rock loading. According to the information entropy calculation method in probability statistics, it is assumed that all possible distributions of results satisfy the following probability conditions:

$$0 \leq \delta_i \leq 1 \quad (i = 1, 2, \dots, n), \quad (6)$$



$$\sum_{i=1}^n \delta_i = 1, \tag{7}$$

$$H(x) = H(\delta_1, \delta_2, \dots, \delta_n) = - \sum_{i=1}^n \delta_i \log \delta_i. \tag{8}$$

Normalizing the entropy value,

$$H(t) = H(x) / \log N, \tag{9}$$

where  $H(x)$  represents the entropy value;  $N$  represents all grade states in the whole system, and every 5 dB is a level in the acoustic emission amplitude classification;  $\delta_i$  is the occurrence probability of this state, which is the ratio of the number of acoustic emission events to the total number of events within the same amplitude range;  $H(t)$  is the normalized time entropy.

The entropy value of the acoustic emission event was calculated as follows:

- (a) A Python program was written to divide the time calculation window. Every 1000 s was selected as the calculation window to count the number of acoustic emission events because the cycle elapsed for a long time.
- (b) The acoustic emission amplitude levels were classified in the time period, with a level of every 5 dB, and the distribution of the acoustic emission signals was counted in each level.
- (c) The probability of acoustic emission events was calculated in each window.
- (d) Equations (8) and (9) were used to calculate the entropy value of acoustic emission in the rock cycle loading and unloading stages.

Figure 9 illustrates the stress in the whole process of the cyclic loading and unloading deformation. The failure stress of monzogranite is captured under different confining pressures. The curve of acoustic emission cumulative energy and acoustic emission energy rate with time are correspondingly recorded.

According to the calculation method of the acoustic emission b value, the corresponding Python code was compiled to obtain the variation characteristics of the acoustic emission b value during the whole process of the monzogranite cyclic loading and unloading (Erarslan 2016; Liu and Dai 2021; Martin and Chandler 1994; Yu et al. 2021; Zhang and Zhang 2017; Liu et al. 2021; Wang et al. 2023; Yang et al.

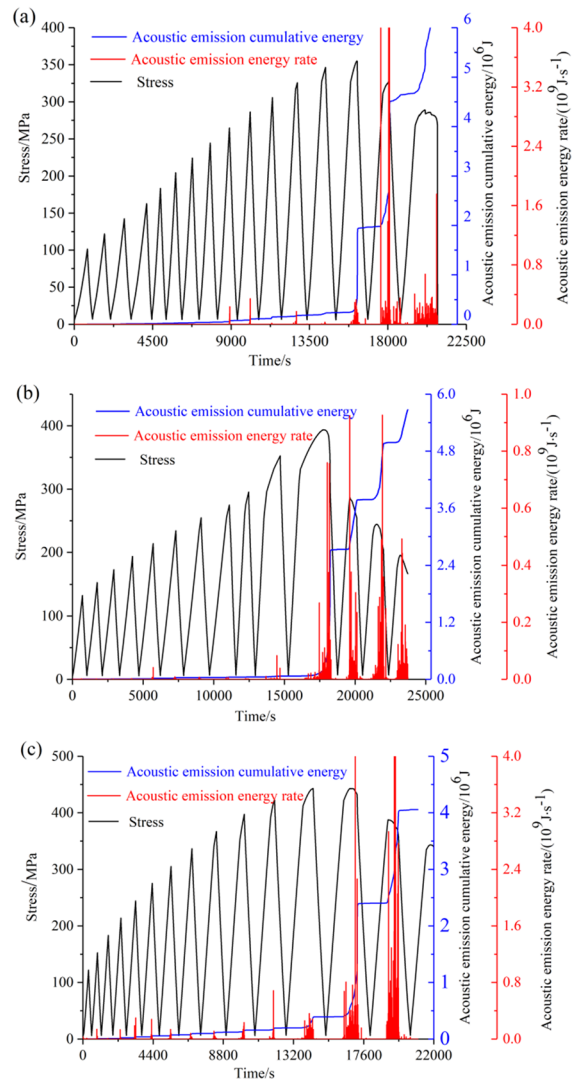


**Fig. 9** Variation curves of acoustic emission cumulative energy and acoustic emission energy rate of rocks under different confining pressures: **a** Confining pressure: 10 MPa; **b** Confining pressure: 20 MPa; **c** Confining pressure: 30 MPa

2022; He 2022). The acoustic emission b value and entropy value curves of the whole deformation process and failure of the monzogranite under different confining pressure cyclic loads were obtained, as illustrated in Fig. 10.

Figures 9 and 10 show that the overall acoustic emission b value curve of the monzogranite failure process exhibited a downward trend while the acoustic emission entropy exhibited a fluctuating upward trend. The change trend of the acoustic emission

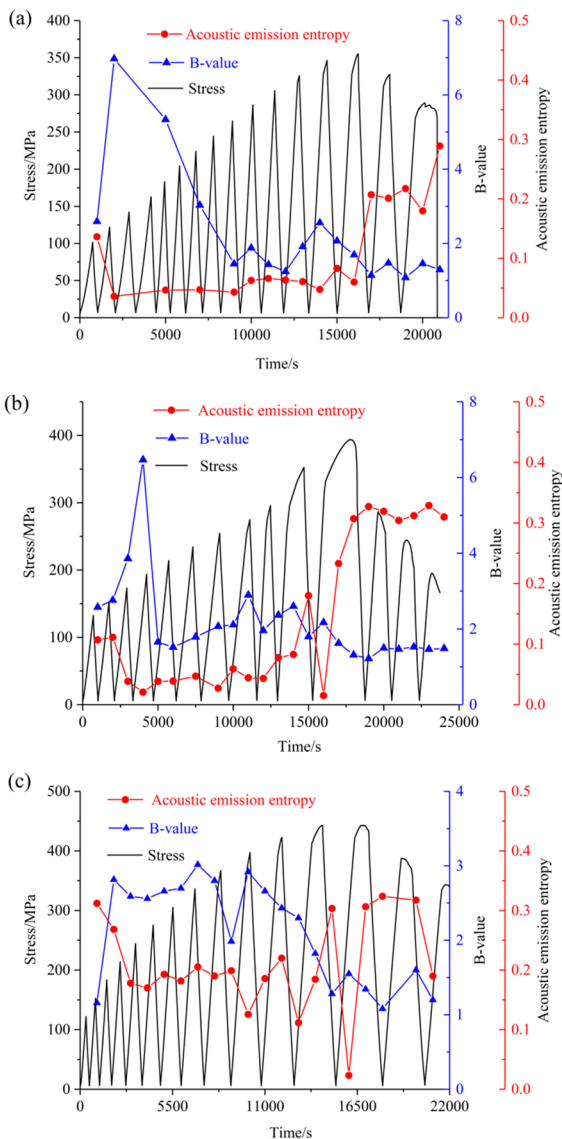


**Fig. 10** Curves of  $b$  and entropy values of acoustic emission of rocks under different confining pressures: **a** Confining pressure: 10 MPa; **b** Confining pressure: 20 MPa; **c** Confining pressure: 30 MPa

$b$  value and that of the acoustic emission entropy value had opposite trends. Compared with the rock samples under 30 MPa confining pressure, the rock samples under the confining pressure of 10 MPa and 20 MPa in the initial stage showed a lower the acoustic emission  $b$  value fluctuated, indicating the acoustic emission behavior inside the rock at this stage. The signal was weak, corresponding to the acoustic emission cumulative energy as illustrated in

**Fig. 9.** The acoustic emission cumulative energy was at a low level, and the rock was in the stage of fissure closure, with mainly small fractures of the same scale. The acoustic emission signal amplitude was relatively close, and the entropy value was relatively high; As the cyclic upper limit stress increased, the rock entered the plastic stage, the acoustic emission  $b$  value began to decrease slowly, larger-scale fractures were gradually generated inside the rock sample, and the acoustic emission signal energy increased. At the internal accumulation stage, the acoustic emission entropy value had a short decline process, the amplitude signal was widely distributed, and the acoustic emission energy rate increased considerably. When the upper limit stress of the rock internal accumulation was close to the peak stress, the acoustic emission was in the quiet period just before the rock rupture. The acoustic emission entropy value decreased sharply, and the entropy value was at the lowest level. When the stress level was equal to the peak stress, the acoustic emission signal had a large, sudden increase in the acoustic emission cumulative energy. The corresponding acoustic emission entropy value rapidly increased to the maximum value. The crack was in an unstable development stage and eventually turned into an unstable failure. The acoustic emission entropy value before and after the rock rupture showed an obvious “V”-shaped change characteristic. The lowest point of the entropy value corresponded to the quiet period of the acoustic emission signal. When the confining pressure was 30 MPa, 20 MPa and 10 MPa, the lowest entropy value was ahead of the rock rupture point at 813.5 s, 625.3 s and 343.5 s, respectively. Therefore, the higher the confining pressure was, the higher the acoustic emission entropy was. The timing point of the lowest value was earlier than the rock rupture point.

## 4 Discussion

Figure 11 shows the schematic diagram of the curve change of the monzogranite time-acoustic emission event number-entropy value-fracture volume strain ratio under different confining pressures. As the stress level increased, the number of the acoustic emission events and fracture volume strain ratio curve of the monzogranite showed an upward trend. This phenomenon showed that under the action of cyclic loading,

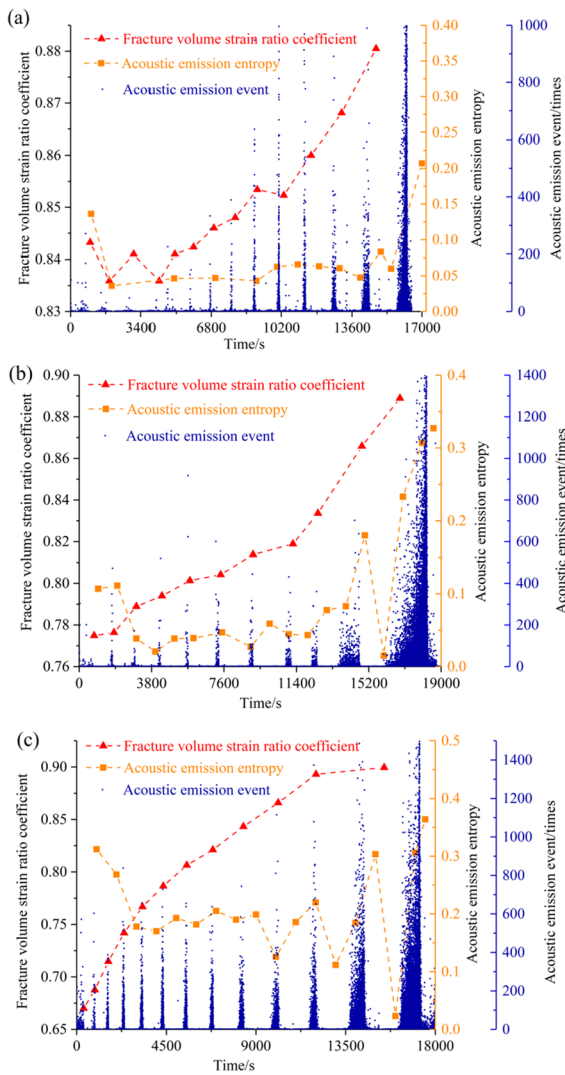


**Fig. 11** Time acoustic emission event number-entropy-volume strain ratio curve of different confining pressures of monzogranite: **a** Confining pressure: 10 MPa; **b** Confining pressure: 20 MPa; **c** Confining pressure: 30 MPa

the relative scale of the fracture volume strain to the total volume strain increased, and the fractures in the rock were constantly developing. The acoustic emission entropy value had an obvious stage division. The acoustic emission entropy value showed a rapid decrease in the crack closure stage, a slow rise in the crack stable development stage, an unstable crack development stage and a post-peak residual deformation stage, and a rapid upward trend. Overall, the

acoustic emission entropy value showed that the more fractures developed in the rock, the larger the acoustic emission entropy value was. Therefore, the acoustic emission entropy value can better reflect the development of the internal fractures in the rock.

The initial loading stage of the rock was the crack closure stage. At this stage, the rock was compressed and closed. The volume strain of the rock was mainly the volume strain of the crack. The acoustic emission entropy value was at a high level. As the stress level increased, the rock entered the elastic deformation stage, the number of acoustic emissions signal events was not obvious, and the entropy value was at a low level. As the stress level continued to increase, the rock entered the crack stable development stage, and the acoustic emission signal and amplitude were generated. The distribution range gradually expanded, and the acoustic emission entropy began to increase slowly. When the stress level was close to the peak strength, the volume strain ratio of the fracture increased rapidly, indicating that the fracture scale increased rapidly at this stage, and the stage was the unstable fracture expansion stage. The acoustic emission signal, amplitude, and entropy value increased gradually. When the stress reached the rock peak intensity, many acoustic emission signal events were generated; the large-scale signal accounted for the main part of the acoustic emission signal, and the acoustic emission entropy value was at a relatively high level. After reaching the peak intensity, the rock entered the post-peak residual deformation stage. A macroscopic fracture surface was formed inside the rock, and the fracture volume strain ratio was close to 1, indicating that the rock fracture volume accounted for the main part of the main total volume strain at this stage.

The acoustic emission entropy value before and after the rock rupture presented a distinct “V”-shaped change, and the lowest point of the “V”-shaped change of the acoustic emission entropy value corresponded to the quiet period of the acoustic emission. Moreover, the higher the confining pressure of the rock was, the greater the mutation degree of the acoustic emission entropy value was, the greater the entropy reduction degree was, and the earlier the rock rupture point was at the lowest point of the acoustic emission entropy value.

## 5 Conclusion

The fissure volume evolution and acoustic emission entropy characteristics of monzogranite under cyclic loading were obtained through triaxial cyclic loading–unloading tests and acoustic emission monitoring analysis for monzogranite taken from a gold mine located in the Jiaodong Peninsula at a depth of – 1600 m. The main conclusions of this study are as follows:

- (1) The fracture volume strain ratio factor is introduced to comprehensively describe the relative relationship between fracture volume strain and total volume strain. The experimental results demonstrate that the fracture volume strain ratio factor can effectively reflect the relative scale of fracture development in the rock. As the stress level increased, the fracture development scale gradually expanded, and the fracture volume strain ratio factor showed an upward trend.
- (2) Under different confining pressures, the volume strain ratios of fractures had different variation characteristics which were obviously determined by confining pressure. As the confining pressure increased, the volume strain ratio curve of the fracture showed three changing characteristics: stable fluctuation, slow rise, and finally rapid rise.
- (3) The acoustic emission entropy value effectively reflected the evolution behavior of crack propagation inside the loaded rock. As the number of the acoustic emission events increased, the acoustic emission entropy value showed a dominant upward trend. The acoustic emission entropy value before and after the rock failure presented a “V”-shaped change. The lowest point of the “V”-shaped change in the acoustic emission entropy value corresponded to the quiet period of the acoustic emission. A higher confining pressure results in a greater the mutation degree of the acoustic emission entropy value. Also, the higher the confining pressure was, the greater the decrease in the entropy value was, and the earlier the rock rupture point was reached.

**Author contributions** L.L. and T.W. wrote the main manuscript text, Z.Z. conducted the experiments, S.Z. modified the manuscript text, J.W. prepared figures. All authors reviewed the manuscript.

**Funding** This work was funded by National Natural Science Foundation of China (Grant Nos. 52004015, 52311530070, and 51874014), the fellowship of China National Postdoctoral Program for Innovative Talents (Grant No. BX2021033), the fellowship of China Postdoctoral Science Foundation (Grant Nos. 2021M700389 and 2023T0025), the Fundamental Research Funds for the Central Universities of China (Grant No. FRF-IDRY-20–003, Interdisciplinary Research Project for Young Teachers of USTB), and State Key Laboratory of Strata Intelligent Control and Green Mining Co-founded by Shandong Province and the Ministry of Science and Technology, China (Grant No. SICGM202108).

**Availability of data and materials** All the data, models or code generated or used in the present study are available from the corresponding author by request.

### Declarations

**Ethics approval and consent to participate** The authors declare that this paper does not involve ethical issues.

**Consent for publication** All authors consent to submit the paper to Geomechanics and Geophysics for Geo-Energy and Geo-Resources.

**Competing interests** The authors declare that they have no known competing financial interests or personal relationships that could have appeared to influence the work reported in this paper.

**Open Access** This article is licensed under a Creative Commons Attribution 4.0 International License, which permits use, sharing, adaptation, distribution and reproduction in any medium or format, as long as you give appropriate credit to the original author(s) and the source, provide a link to the Creative Commons licence, and indicate if changes were made. The images or other third party material in this article are included in the article's Creative Commons licence, unless indicated otherwise in a credit line to the material. If material is not included in the article's Creative Commons licence and your intended use is not permitted by statutory regulation or exceeds the permitted use, you will need to obtain permission directly from the copyright holder. To view a copy of this licence, visit <http://creativecommons.org/licenses/by/4.0/>.

## References

- Akdag S, Karakus M, Nguyen GD, Taheri A, Bruning T (2021) Evaluation of the propensity of strain burst in brittle granite based on post-peak energy analysis. *Underground Space* 6(1):1–11. <https://doi.org/10.1016/j.undsp.2019.08.002>

- Bressan G, Barnaba C, Gentili S, Rossi G (2017) Information entropy of earthquake populations in northeastern Italy and western Slovenia. *Phys Earth Planet Inter* 271:29–46. <https://doi.org/10.1016/j.pepi.2017.08.001>
- Cai M, Kaiser PK, Tasaka Y, Maejima T, Morioka H, Minami M (2004) Generalized crack initiation and crack damage stress thresholds of brittle rock masses near underground excavations. *Int J Rock Mech Min Sci* 41(5):833–847
- Chen Y, Zuo JP, Li ZH, Dou R (2020) Experimental investigation on the crack propagation behaviors of sandstone under different loading and unloading conditions. *Int J Rock Mech Min Sci* 130:104310. <https://doi.org/10.1016/j.ijrmms.2020.104310>
- Duan YT, Li X, Zheng B, Li X, Zheng B, He JM, Hao J (2019) Cracking evolution and failure characteristics of Longmaxi shale under uniaxial compression using real-time computed tomography scanning. *Rock Mech Rock Eng* 52(9):3003–3015. <https://doi.org/10.1007/s00603-019-01765-0>
- Erarslan N (2013) A study on the evaluation of the fracture process zone in CCNBD rock samples. *Exp Mech* 53(8):1475–1489. <https://doi.org/10.1007/s11340-013-9750-5>
- Erarslan N (2016a) Microstructural investigation of subcritical crack propagation and fracture process zone (FPZ) by the reduction of rock fracture toughness under cyclic loading. *Eng Geol* 208:181–190. <https://doi.org/10.1016/j.enggeo.2016.04.035>
- Erarslan N (2016b) Microstructural investigation of subcritical crack propagation and Fracture Process Zone (FPZ) by the reduction of rock fracture toughness under cyclic loading. *Eng Geol* 208:181–190. <https://doi.org/10.1016/j.enggeo.2016.04.035>
- Ghamgosar M, Erarslan N (2016) Experimental and Numerical studies on development of fracture process zone (FPZ) in rocks under cyclic and static loadings. *Rock Mech Rock Eng* 49(3):893–908. <https://doi.org/10.1007/s00603-015-0793-z>
- Ghasemi S, Khamsehchiyan M, Taheri A, Nikudel MR, Zaloli A (2020) Crack evolution in damage stress thresholds in different minerals of granite rock. *Rock Mech Rock Eng* 53:1163–1178. <https://doi.org/10.1007/s00603-019-01964-9>
- Harte D, Vere-Jones D (2005) The entropy score and its uses in earthquake forecasting. *Pure Appl Geophys* 162:1229–1253
- He M (2022) The future of rock mechanics lies with China: inaugural editorial for *Rock Mechanics Bulletin*. *Rock Mech Bull* 1(1):100010. <https://doi.org/10.1016/J.ROCKMB.2022.100010>
- Hoek E, Martin CD (2014) Fracture initiation and propagation in intact rock—A review. *J Rock Mech Geotech Eng* 6(4):287–300. <https://doi.org/10.1016/j.jrmge.2014.06.001>
- Ji HG, Zhang YZ, Jin Y (2012) Experimental study of confining pressure effect on acoustic emission characteristics of monzonite granite under triaxial compression. *Chin J Rock Mech Eng* 31(6):1162–1168
- Ju Y, Xi C, Zhang Y, Mao LT, Gao F, Xie HP (2018) Laboratory in situ CT observation of the evolution of 3D fracture networks in coal subjected to confining pressures and axial compressive loads: a novel approach. *Rock Mech Rock Eng* 51(11):3361–3375. <https://doi.org/10.1007/s00603-018-1459-4>
- Liu Y, Dai F (2021) A review of experimental and theoretical research on the deformation and failure behavior of rocks subjected to cyclic loading. *J Rock Mech Geotech Eng* 13(5):1203–1230. <https://doi.org/10.1016/J.JRMGE.2021.03.012>
- Liu LY, Ji HG, Elsworth D, Zhi S, Lv XF, Wang T (2020a) Dual-damage constitutive model to define thermal damage in rock. *Int J Rock Mech Min Sci* 126:104185. <https://doi.org/10.1016/j.ijrmms.2019.104185>
- Liu LY, Ji HG, Wang T, Pei F, Quan DL (2020b) Mechanism of country rock damage and failure in deep shaft excavation under high pore pressure and asymmetric geostress. *Chin J Eng* 42(06):715–722. <https://doi.org/10.13374/j.issn2095-9389.2019.11.05.004>
- Liu LY, Ji HG, Lü XF, Wang T, Zhi S, Pei F, Quan DL (2021) Mitigation of greenhouse gases released from mining activities: a review. *Int J Miner Metall Mater* 28:513–521. <https://doi.org/10.1007/S12613-020-2155-4>
- Liu LY, Zhang L, Ji HG (2022) Mechanism analysis of rock damage and failure based on relation between deep cavern axial variation and in situ stress field. *Chin J Eng* 44(4):516–525. <https://doi.org/10.13374/j.issn2095-9389.2021.04.09.003>
- Ma LJ, Liu XY, Wang MY, Xu HF, Hua RP, Fan PX, Jiang SR, Wang GA, Yi QK (2013) Experimental investigation of the mechanical properties of rock salt under triaxial cyclic loading. *Int J Rock Mech Min Sci* 62:34–41. <https://doi.org/10.1016/j.ijrmms.2013.04.003>
- Ma Q, Liu X, Tan Y, Elsworth D, Shang J, Song D, Liu XS, Yan FY (2023) Numerical study of mechanical properties and microcrack evolution of double-layer composite rock specimens with fissures under uniaxial compression. *Eng Fract Mech* 289(2):109403. <https://doi.org/10.1016/j.engfractmech.2023.109403>
- Martin CD, Chandler NA (1994) The progressive fracture of Lac du Bonnet granite. *Int J Rock Mech Min Sci Geomech Abstr* 31(6):643–659
- Meng QB, Liu JF, Li R, Pu H, Chen YL (2021) Experimental study on rock strength and deformation characteristics under triaxial cyclic loading and unloading conditions. *Rock Mech Rock Eng* 54:777–797. <https://doi.org/10.1007/s00603-020-02289-8>
- Momeni A, Karakus M, Khanlari GR, Heidari M (2015) Effects of cyclic loading on the mechanical properties of a granite. *Int J Rock Mech Min Sci* 77:89–96. <https://doi.org/10.1016/j.ijrmms.2015.03.029>
- Qiu SL, Feng XT, Xiao JQ, Zhang CQ (2014) An experimental study on the pre-peak unloading damage evolution of marble. *Rock Mech Rock Eng* (2) 47(2):401–419. <https://doi.org/10.1007/s00603-013-0394-7>
- Taheri A, Royle A, Yang Z, Zhao Y (2016) Study on variations of peak strength of a sandstone during cyclic loading. *Geomech Geophys Geo-Energy Geo-Resour* 2:1–10. <https://doi.org/10.1007/s40948-015-0017-8>
- Wang Y, Feng WK, Hu RL, Li CH (2021) Fracture evolution and energy characteristics during marble failure under triaxial fatigue cyclic and confining pressure unloading (FC-CPU) conditions. *Rock Mech Rock Eng* 54:799–818. <https://doi.org/10.1007/s00603-020-02299-6>

- Wang T, Ye WW, Tong YM, Jiang NS, Liu LY (2023) Residual stress measurement and analysis of siliceous slate-containing quartz veins. *Int J Miner Metall Mater*. <https://doi.org/10.1007/s12613-023-2667-9>
- Xiao JQ, Ding DX, Jiang FL, Xu G (2009) Fatigue damage variable and evolution of rock subjected to cyclic loading. *Int J Rock Mech Min Sci* 47(3):461–468
- Xu T, Fu M, Yang S, Heap MJ, Zhou G (2021) A Numerical Meso-scale elasto-plastic damage model for modeling the deformation and fracturing of sandstone under cyclic loading. *Rock Mech Rock Eng* 54:4569–4591. <https://doi.org/10.1007/s00603-021-02556-2>
- Yang SQ, Tian WL, Ranjith PG, Liu XR, Chen M, Cai W (2022) Three-dimensional failure behavior and cracking mechanism of rectangular solid sandstone containing a single fissure under triaxial compression. *Rock Mech Bull* 1(1):100008. <https://doi.org/10.1016/J.ROCKMB.2022.100008>
- Yu J, Liu ZH, Lin LH, Huang JG, Ren WB, Zhou L (2021) Characteristics of dilatancy of marble under variable amplitude cyclic loading and unloading. *Rock Soil Mech* 42(11):2934–2942. <https://doi.org/10.16285/j.rsm.2021.0256>
- Zhang Q, Zhang XP (2017) A numerical study on cracking processes in limestone by the b-value analysis of acoustic emissions. *Comput Geotech* 92:1–10. <https://doi.org/10.1016/j.compgeo.2017.07.013>
- Zhang R, Xie HP, Liu JF, Deng J, Peng Q (2006) Experimental study on acoustic emission characteristics of rock failure under uniaxial multilevel loadings. *Chin J Rock Mech Eng* 25(12):2584–2588
- Zhang GK, Li HB, Wang MY, Li XF (2019) Crack propagation characteristics in rocks containing single fissure based on acoustic testing and camera technique. *Rock Soil Mech* 40(S1):63–7281
- Zhou XP, Zhao Z, Liu Y (2020) Digital spatial cracking behaviors of fine-grained sandstone with precracks under uniaxial compression. *Int J Numer Anal Meth Geomech* 44:1770–1787

**Publisher's Note** Springer Nature remains neutral with regard to jurisdictional claims in published maps and institutional affiliations.